Journal of Sedimentary Research

Journal of Sedimentary Research, 2019, v. 89, 242–252
Research Article
DOI: http://dx.doi.org/10.2110/jsr.2019.15

EVOLUTION OF THE ZONAL GRADIENTS ACROSS THE EQUATORIAL PACIFIC DURING THE MIOCENE–PLEISTOCENE

CATHERINE BELTRAN,*[1] GABRIELLE ROUSSELLE,[1] MARC DE RAFÉLIS,[2] MARIE-ALEXANDRINE SICRE,[3] NATHALIE LABOURDETTE,[1] AND STEFAN SCHOUTEN[4,5]

[1]Sorbonne Universités (UPMC, Université Paris 06), UMR 7193, ISTeP, Case Postale 116-4, place Jussieu 75005 Paris, France
[2]Université Paul Sabatier, UMR 5563, Géosciences Environnements Toulouse-14, avenue Edouard Belin, 31400 Toulouse, France
[3]Sorbonne Universités (UPMC, Université Paris 06)-CNRS-IRD-MNHN, LOCEAN Laboratory, 4 place Jussieu, F-75005 Paris, France
[4]NIOZ Royal Netherlands Institute for Sea Research, Department of Marine Microbiology and Biogeochemistry, and University of Utrecht, P.O. Box 59, 1790 AB Den Burg (Texel), The Netherlands
[5]Departement of Earth Sciences, Utrecht University, Heidelberglaan 8, 3584 CS Utrecht, The Netherlands
e-mail: catherine.beltran@otago.ac.nz

ABSTRACT: Combining $U^{k'}_{37}$ - and TEX_{86}-derived temperatures and oxygen isotopic values of mixed-layer and thermocline species from the IODP site U1338 (East Equatorial Pacific) and ODP Site 806 (West Equatorial Pacific) we assess the evolution of the zonal sea-surface temperature gradients and thermocline depth across the equatorial Pacific from the late Miocene through the Pleistocene. Data suggest a long-term shoaling of the thermocline along the equator throughout the Miocene–Pliocene that accelerated around 5.3 Ma. We identify a critical transition at about 3.8 Ma from a El-Niño-like-dominated mean state during the late Miocene and early Pliocene to a La-Niña-like-dominated state during the late Pliocene–Pleistocene. This transition coincides with the restriction of the Indonesian seaway and the onset of ice growth in the northern hemisphere and in Antarctica that led to the long-term strengthening of the Walker circulation and affected low-latitude zonal gradient.

INTRODUCTION

The equatorial Pacific Ocean plays an important role in the global climate by influencing the heat transport from low to mid- and high latitudes. The modern structure of the equatorial Pacific is characterized by a pronounced east–west asymmetry of the thermocline depth and of sea-surface temperature (SSTs) with the warm pool ($\sim$ 29°C) in the west and the cold tongue ($\sim$ 23°C) in the east (Fig. 1). The thermocline in the West Equatorial Pacific is deep and controls the flux of atmospheric latent heat (Tian et al. 2001) whereas in the east it is shallow and heat is absorbed (Boccaletti et al. 2004). The SSTs across the equatorial Pacific are affected by the El Niño–Southern Oscillation (Cane 1998), one of the most important components of the global climate system, which alternates at inter-annual time scales between warm "El Niño" and cold "La Niña" phases.

The El Niño–Southern Oscillation is sensitive to the SST distribution across the equatorial Pacific through the link between temperatures and the strength of the trade winds (Neelin et al. 1998). Changes in the meridional SST gradient in the equatorial Pacific have important consequences on the local and global climate.

The modern setting of the equatorial Pacific was established during the mid- to late Miocene (LaRivière et al. 2012) through the progressive closure of the Central American Seaway (CAS) and the Indonesian Seaway (Keigwin 1982; Haug and Tiedemann 1998; Srinivasan and Sinha 1998; Schneider and Schmittner 2006) together with Northern Hemisphere Glaciation (Mudelsee and Raymo 2005) (Fig. 2). During this period, the onset of the modern thermohaline circulation and equatorial upwelling led to the progressive cooling of deep-water (Woodruff and Savin 1989; Ravelo et al. 2004), upper-ocean stratification, and thermocline rise. Nathan and Leckie (2009) dated the proto warm pool in the West Equatorial Pacific (WEP) between 11.6 and 10 Ma. The thermocline depth asymmetry set up around 4.8 Ma and induced a well-documented cold-water tongue in the Eastern Equatorial Pacific (EEP) between 4.4 and 3.6 Ma (Chaisson and Ravelo 2000; Wara et al. 2005; Steph et al. 2010; Rousselle et al. 2013).

Although numerous studies (e.g., Raymo et al. 1996; Haywood and Valdes 2004; Ravelo et al. 2004, 2006; Rickaby and Halloran 2005; Wara et al. 2005; Barreiro et al. 2005; Fedorov et al. 2006, 2013; Dekens et al. 2008; Brierley et al. 2009) established that the equatorial Pacific zonal gradients were weaker during the early Pliocene warm period (El Niño-like, El Padre) and stronger during the mid-Holocene (La Niña-like; Koutavas et al. 2006), there is no consensus on the long-term evolution of the equatorial Pacific mean state since the Miocene (Fig. 2). This is a major limitation to predict El Niño–Southern Oscillation, in that its behavior is closely related to long-term changes in tropical Pacific oceanography that are still not fully understood. Some authors suggest that the equatorial thermal state remained unchanged over the last 12 Myr (Zhang et al. 2014) whereas others identified alternating El Niño-like and La Niña-like conditions (Wara et al. 2005; Ravelo et al. 2006; Nathan and Leckie 2009; Kamikuri et al. 2009; Drury et al. 2018) or a progressive shoaling of the thermocline over the last 13 Myr (LaRiviere et al. 2012).

* Department of Marine Science, University of Otago, P.O. Box 56, Dunedin 9054, New Zealand

Published Online: March 2019
 1527-1404/19/089-242

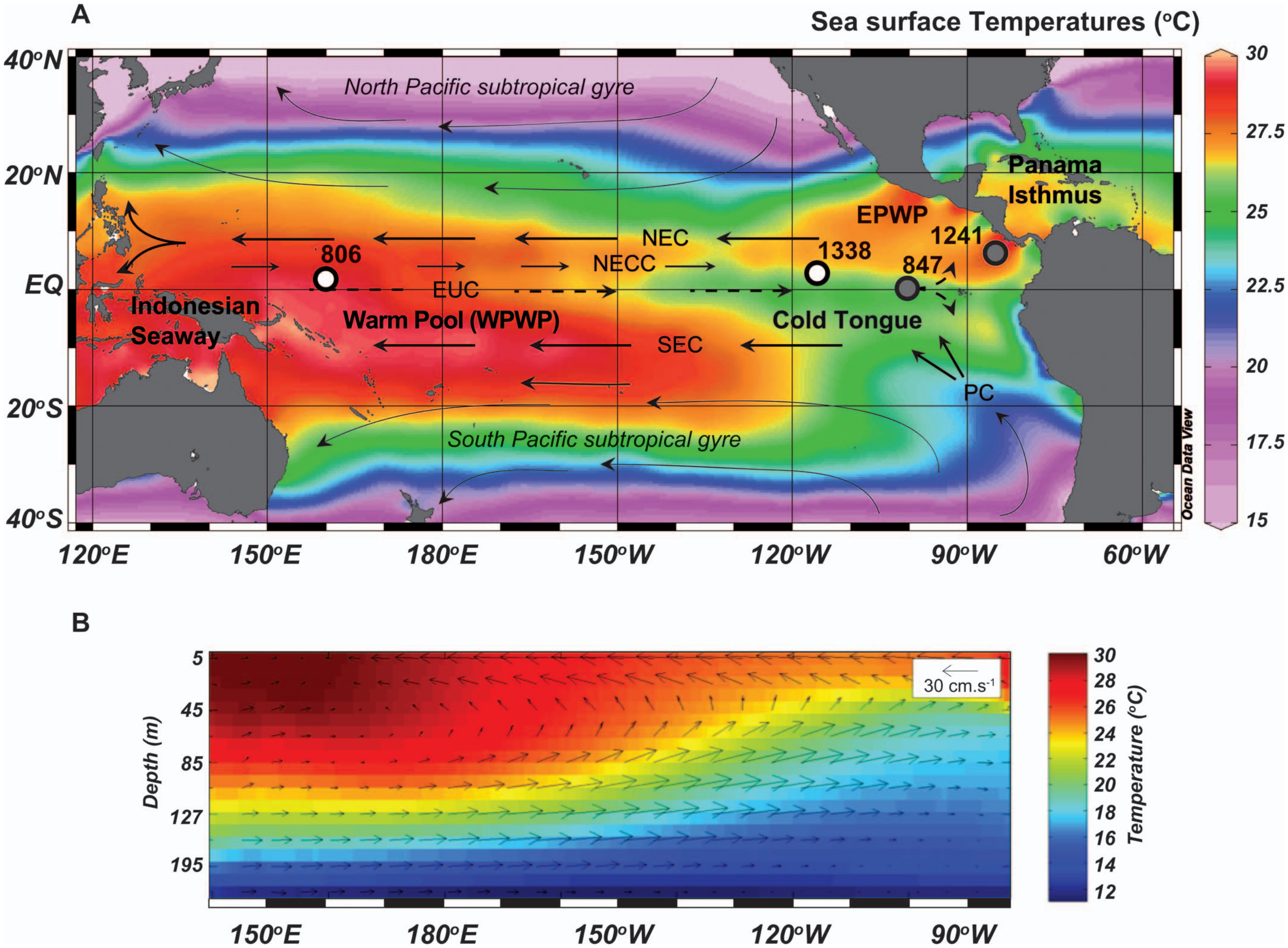

FIG. 1.—**A)** Modern equatorial Pacific sea-surface temperatures (SSTs) from Ocean Data View. The white dots show the location of the study sites, ODP 806 and IODP U1338. The gray dots indicate the sites of previously published oxygen-isotope records (ODP 847 and 1241). WPWP, Western Pacific Warm Pool; EPWP, Eastern Pacific Warm Pool; NEC, North Equatorial Current; SEC, South Equatorial Current; EUC, Equatorial Under Current; NECC, North Equatorial Counter Current, PC, Peru Current (modified after Pisias et al. 1995). **B)** Cross sections of temperature (colors) and currents (vectors) averaged over 2.5°S–2.5°N (modified after US CLIVAR).

Because the past variability of the equatorial Pacific mean state is also considered to have played a role in major climatic transitions (Yin and Battisti 2001), reconstructing the long-term evolution of the thermal structure in this region is crucial.

While most published studies focus on very specific time intervals (e.g., Medina-Elizalde and Lea 2010; Ford et al. 2015), the purpose of this study is to examine the long-term evolution of equatorial Pacific surface conditions over the last 10 Myr. To do so, surface and subsurface temperature records from IODP Site U1338 (EEP) (Fig. 1) are generated from both alkenones ($U^{K'}_{37}$) produced by coccolithophores (marine unicellular haptophyte algae, Brassell et al. 1986) and glycero-dialkyl glycerol-tetraethers (GDGTs, TEX^{H}_{86}) produced by *Thaumarchaeota* (Archaea, Schouten et al. 2002; Kim et al. 2010). Additional hydrological information is provided by the oxygen-isotope composition of calcareous nannofossils *Noelaerhabdaceae* spp. calcifying in the photic zone and the thermocline-dweller foraminifera *Globorotalia menardii* (Martin 1999; Spero et al. 2003) recovered from the ODP Site 806 (WEP) and IODP Site U1338 (Fig. 1).

OCEANOGRAPHIC SETTING

The equatorial Pacific surface ocean circulation, controlled by the Walker cell and trade winds, results in two westward surface currents, the North and South Equatorial Currents, respectively (SEC and NEC; Fig. 1). The easterly winds pile warm waters in the WEP and create a subsurface eastward circulation known as the Equatorial Under Current (EUC), which brings cold and nutrient-rich waters to the surface in the EEP. The subsequent thinning of the mixed-layer and formation of a cold tongue in the EEP produce a strong W–E asymmetry of the equatorial thermocline depth, deeper in the West Pacific than in the East Pacific (Fig. 1). The modern equatorial SST gradient across the Pacific varies in response to the inter-annual El Nino–Southern Oscillation. During El Niño years, the trade winds weaken, the thermocline deepens in the EEP, and the equatorial upwelling attenuates. As a consequence, the equatorial SST gradient is reduced, mean temperatures are warmer, and the extratropical heat distribution is impacted (Molnar and Cane 2002; McPhaden et al. 2006).

Since the Miocene, the Pacific zonal temperature gradients and the thermocline tilt have varied. Extended periods of reduced equatorial SST

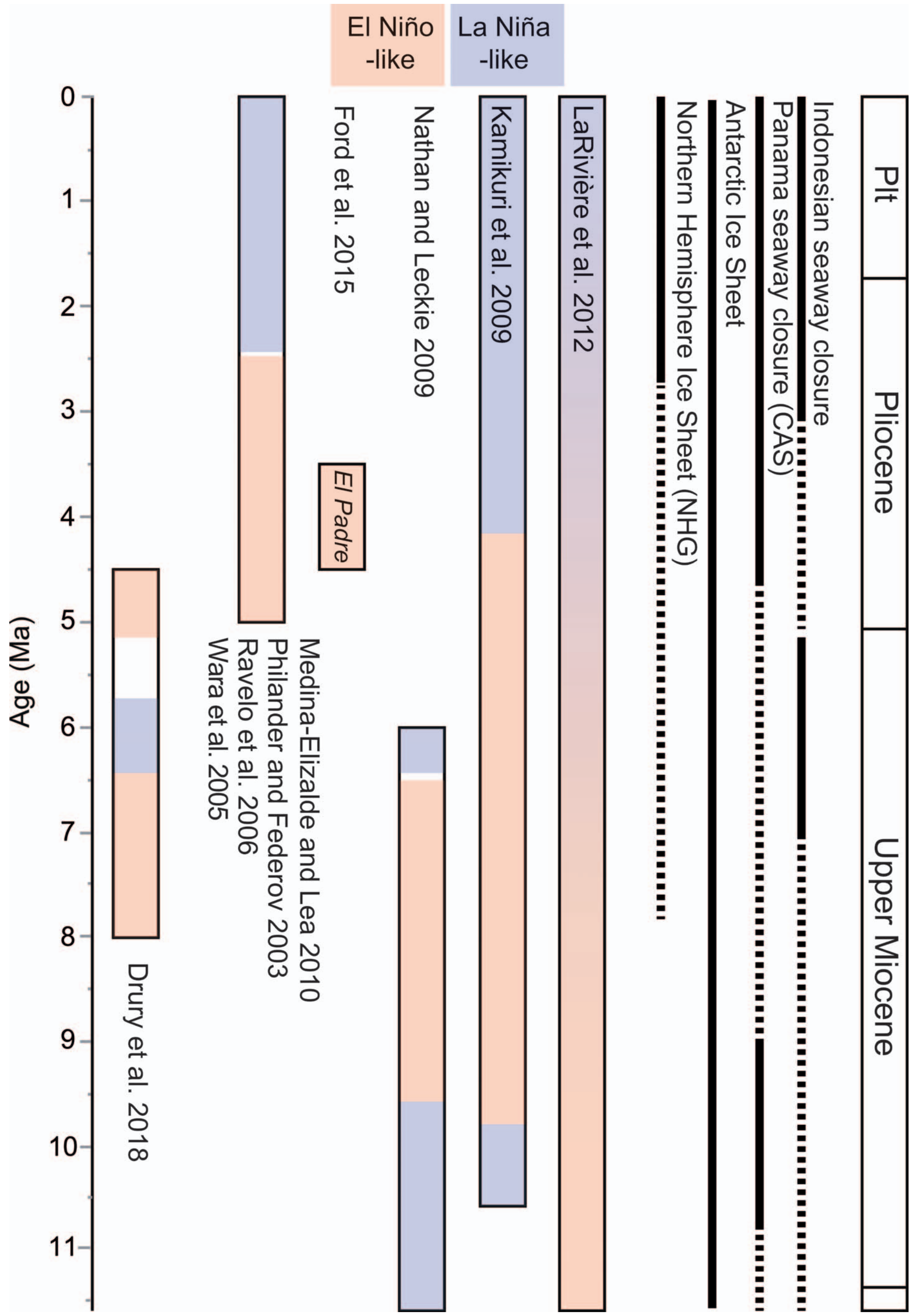

FIG. 2.—Comparison of El Niño-like (in red) and La Niña-like (in blue) time periods inferred from previous studies using different proxies from the EEP and WEP over the past 12 Myrs.

gradient and deep thermocline that mimic the modern El Niño events are called permanent El Niño-like states. Similarly, periods of long-term strong equatorial Pacific zonal gradients are called La Niña-like states.

MATERIALS AND METHODS

IODP Site U1338 and ODP Site 806

The IODP Site U1338 (2° 30.469′ N, 117° 58.178′ W, 4200 meters water depth, leg 321) was drilled in the EEP, in the modern cold tongue (Pälike et al. 2010) (Fig. 1). Despite the northward drift of the Pacific plate, this site remained in the equatorial band for the past 10 Myr (Pälike et al. 2010). Sediments at Site U1338 were deposited above the calcite compensation depth (Pälike et al. 2012) and are composed of well-preserved biogenic material, predominantly nannofossil oozes, with variable abundances of diatoms, radiolarians, and foraminifera (Pälike et al. 2010). The age model of the core was constructed from biostratigraphic (nannofossils, foraminifers, diatoms, and radiolarians) and paleomagnetic data (Pälike et al. 2010; Backman et al. 2016). Average sedimentation rates are relatively high for the studied time interval (~ 27 m/Myr).

ODP Site 806 (0° 19,1′ N, 159° 21,7′ E, 2520 meters water depth, leg 130) is located on the northeast margin of the Ontong Java plateau in the area of the WEP warm pool (Fig. 1). Sediments are composed mostly of well-preserved calcareous nannofossils and planktic foraminifera. The age model is based exclusively on biostratigraphic data of calcareous nannofossils, foraminifera, diatoms, and radiolarians established by Kroenke et al. (1991), later refined by Takayama (1993) and Chaisson and Leckie (1993). Ages are corrected based on biostratigraphic data of Backman et al. (2016) (see Supplemental Material). The average sedimentation rate at this site is higher than at U1338, ranging from ~ 45 m/Myr between 9 and 5 Ma to ~ 29 m/Myr during the Pliocene.

Proxy records at both sites are generated for the period between 10 and 0.18 Ma using samples from sections U1338B-22H7W through U1338B-1H2W and sections 806B-37X3W through 806B-1H1W. The average sampling resolution of these records varies between 100 kyr and 400 kyr.

Oxygen Stable-Isotope Measurements

To determine changes in the thermocline depth in the EEP and WEP through time, we measured the oxygen-isotope ratios ($\delta^{18}O$) in the calcite of calcareous-nannofossil-enriched fractions and of the upper-thermocline-dweller planktonic foraminifera *Globorotalia menardii*. Calcareous nannofossils calcify mainly in the photic zone and thus are used to derive surface-water properties (Roth 1986) whereas *G. menardii* is selected to assess subsurface water changes.

$\delta^{18}O$ values are measured on calcareous nannofossils *Noelaerhabdaceae* spp. isolated from the bulk sediment following the procedure of Minoletti et al. (2009). $\delta^{18}O$ measurements are performed on the 2–5 μm fractions at both sites. For site U1338, we use the $\delta^{18}O$ data previously published by Rousselle et al. (2013) based on the same protocol as in the present study. $\delta^{18}O$values are measured using a Finnigan Delta E mass spectrometer at 50°C, at a temporal resolution of 400 kyr. The quality of the granulometric separation based on 200 particles counted in smear slides is estimated to be at least 75% except between 8 and 9 Ma at Site 806, where *Sphenolitus abies* dominated. These measurements are thus not considered here.

In addition, five to seven specimens of *G. menardii* were hand-picked from the > 160 μm fractions for isotopic measurements. Analyses are performed on a VG ISOPRIME at 90°C with a precision of 0.1‰ and expressed with reference to the VPDB international standard. Fourty-five samples at Site U1338 and 99 samples at Site 806 were analyzed. The average temporal resolution over the last 10 Myr is between 120 and 150 ka.

Alkenone Analyses

Alkenone-derived SSTs of Site U1338 previously reported by Rousselle et al., (2013) are supplemented in the present study with 23 additional samples selected from the Pliocene interval (U1338B-8H5W to U1338B-1H2W) to reach a temporal resolution of 100 kyr. Sedimentary alkenones are analyzed following the procedure described by Ternois et al. (2000). About 5 g of freeze-dried sediments are extracted in a mixture of CH_2Cl_2 / CH_3OH. Alkenones are isolated from the total lipid extract by silica-gel chromatography using solvents of increasing polarity. The fraction containing alkenones is concentrated, transferred into clean glass vials, and evaporated under a nitrogen stream. Gas-chromatography analyses are performed using a Varian 3400CX series equipped with a septum programmable injector (SPI) and a flame ionization detector (FID). We use a fused silica capillary column (Chrompack CP Sil5CB, 50 m long, 0.32 mm internal diameter, 0.25 μm film thickness) and helium as a carrier gas. The alkenone unsaturation ratio $U^{k'}_{37}$ ($C_{37:2}/(C_{37:2}+C_{37:3})$) is converted into SSTs using the Conte et al. (2006) calibration: $T = -0.957 + 54.293 (U^{k'}_{37}) - 52.894 (U^{k'}_{37})^2 + 28.321 (U^{k'}_{37})^3$, which provides more accurate estimates in the warm-temperature range than Prahl et al. (1988). Average external precision of the SSTs using this calibration has been estimated at ~ 1.2°C (Conte et al. 2006). Replicate analyses indicate internal precision of ± 0.5°C. Because of the limited amount of sediment material at Site 806 (where alkenone concentrations are extremely low), previously published data from Pagani et al. (2010) provide data covering the past 5 Myr. Note that we recalculated SSTs from the$U^{k'}_{37}$values of Pagani et al. (2010) using the Conte et al. (2006) calibration to avoid calibration bias between sites (see Supplemental Material).

GDGT Analyses

Forty samples from Site U1338 were analyzed for GDGTs at the Netherlands Institute for Sea Research (NIOZ, Texel, The Netherlands). About 5 g of sediment are freeze dried and extracted in a mixture of CH_2Cl_2 and CH_3OH. The total lipid extracts are separated following the protocol described in Schouten et al. (2002), using Al_2O_3 column chromatography to separate non-polar compounds from the polar GDGTs. Polar fractions are then filtered through a 0.4 μm pore-size filter, evaporated under nitrogen, and diluted to a concentration of 2 mg/ml. GDGTs are analyzed using an Agilent HP1100 (HPLC) equipped with a Prevail Cyano column (3 μm, 150 mm × 2.1 mm) following Schouten et al. (2007). The TEX_{86} index is calculated using peak areas of the following GDGTs as defined by Schouten et al. (2002): $TEX_{86} = [GDGT2] + [GDGT3] + [GDGT5'] / [GDGT1] + [GDGT2] + [GDGT3] + [GDGT5']$. The TEX^H_{86}, defined as the log(TEX_{86}), is used to calculate temperatures over the past 9 Myr. Temperatures are calculated using the calibration established for temperatures above 15°C by Kim et al. (2010) ($T = 68.4*TEX^H_{86} + 38.6$). The error on temperature estimates is ± 2.5°C. Other calibrations have been proposed for TEX_{86} temperatures, in particular based on Bayesian statistics (Tierney and Tingley 2015) but these yield results similar to those shown here, whereas the Kim et al. (2010) calibration is consistent with other studies from this area (e.g., Seki et al. 2010; Zhang et al. 2014). TEX^H_{86}-derived temperatures are obtained at a mean temporal resolution of 230 kyr. At Site 806, because of the very low GDGT concentrations, we use previously published data from Zhang et al. (2014) covering the past 12 Myr for comparison with the data from Site U1338.

RESULTS

Stable Isotopes of the Calcareous Nannofossil Fine Fractions and G. menardii

$\delta^{18}O$ Record at Site U1338.—The oxygen stable-isotope signatures of the *Noelaerhabdaceae*-enriched fine fractions ($\delta^{18}O_{Noelaerhabdaceae}$) vary between –1.5‰ and 0.5‰ (Fig. 3A). $\delta^{18}O_{Noelaerhabdaceae}$ progressively increase between 8 Ma and 5 Ma, before declining to –1.3‰ until 2.7 Ma and rising again to 0.4‰. The $\delta^{18}O_{Noelaerhabdaceae}$ record is similar to the higher resolution $\delta^{18}O$ record of the surface dweller *G. sacculifer* from the nearby Site 847 covering only the last 5 Myr (Wara et al. 2005) (Figs. 1, 3A).

$\delta^{18}O$ values measured on the thermocline-dwelling planktonic foraminifera *G. menardii* ($\delta^{18}O_{G.menardii}$) over the last 8 Myr (Fig. 3A) demonstrate that values vary between –1.4‰ and 1.25‰ and display trends similar to those of $\delta^{18}O_{Noelaerhabdaceae}$ until 5 Ma. Then, $\delta^{18}O_{G.menardii}$ become more positive than $\delta^{18}O_{Noelaerhabdaceae}$ and still increase until 0.4 Ma, as also recorded in the deep thermocline dweller *G. tumida* $\delta^{18}O$ values ($\delta^{18}O_{G.tumida}$) at Site 847 (Figs. 1, 3A; Wara et al. 2005).

$\delta^{18}O$ Record at Site 806.—$\delta^{18}O_{Noelaerhabdaceae}$ at site 806 vary within a range similar (between –2.8 and 0.9‰) to site U1338 (Fig. 3B).

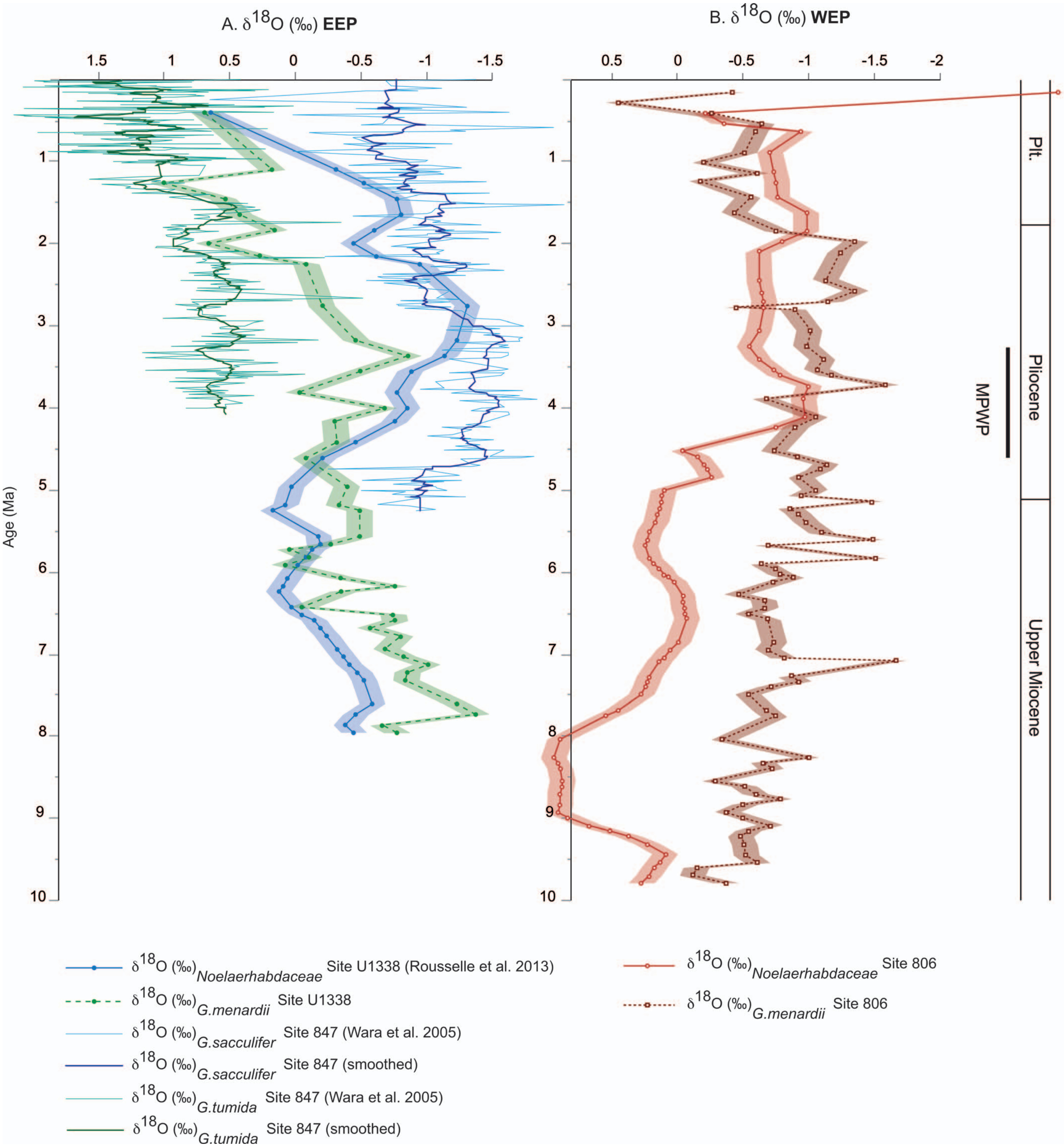

FIG. 3.—**A**) δ^{18}O records in the EEP. $\delta^{18}O_{Noelaerhabdaceae}$ at IODP Site U1338 from Rousselle et al. (2013), $\delta^{18}O_{G.\ sacculifer}$ and $\delta^{18}O_{G.\ tumida}$ at site 847 from Wara et al. (2005), $\delta^{18}O_{G.\ menardii}$ at Site U1338. **B**) δ^{18}O records in the WEP. $\delta^{18}O_{Noelaerhabdaceae}$ and $\delta^{18}O_{G.\ menardii}$ at ODP Site 806.

$\delta^{18}O_{Noelaerhabdaceae}$ values are relatively stable (around 0‰) between 7 Ma and 4.4 Ma and rapidly decline to more negative values between 4.5 Ma and 4 Ma, after which values remain stable until 0.38 Ma. The $\delta^{18}O_{G.menardii}$ record at Site 806 shows a long-term decrease between 9.7 Ma and 7 Ma and becomes stable until 1.9 Ma. At 3.7 Ma oxygen-isotope values decrease sharply by 1‰, and again between 2.5 Ma and 1.8 Ma. The $\delta^{18}O_{G.menardii}$ values then increase to higher values (–0.4 ‰) until 0.5 Ma and further to 0.5‰ at 0.2 Ma. Overall, $\delta^{18}O_{Noelaerhabdaceae}$ and $\delta^{18}O_{G.menardii}$ reveal more positive values in the EEP than in the WEP and include larger-amplitude variations.

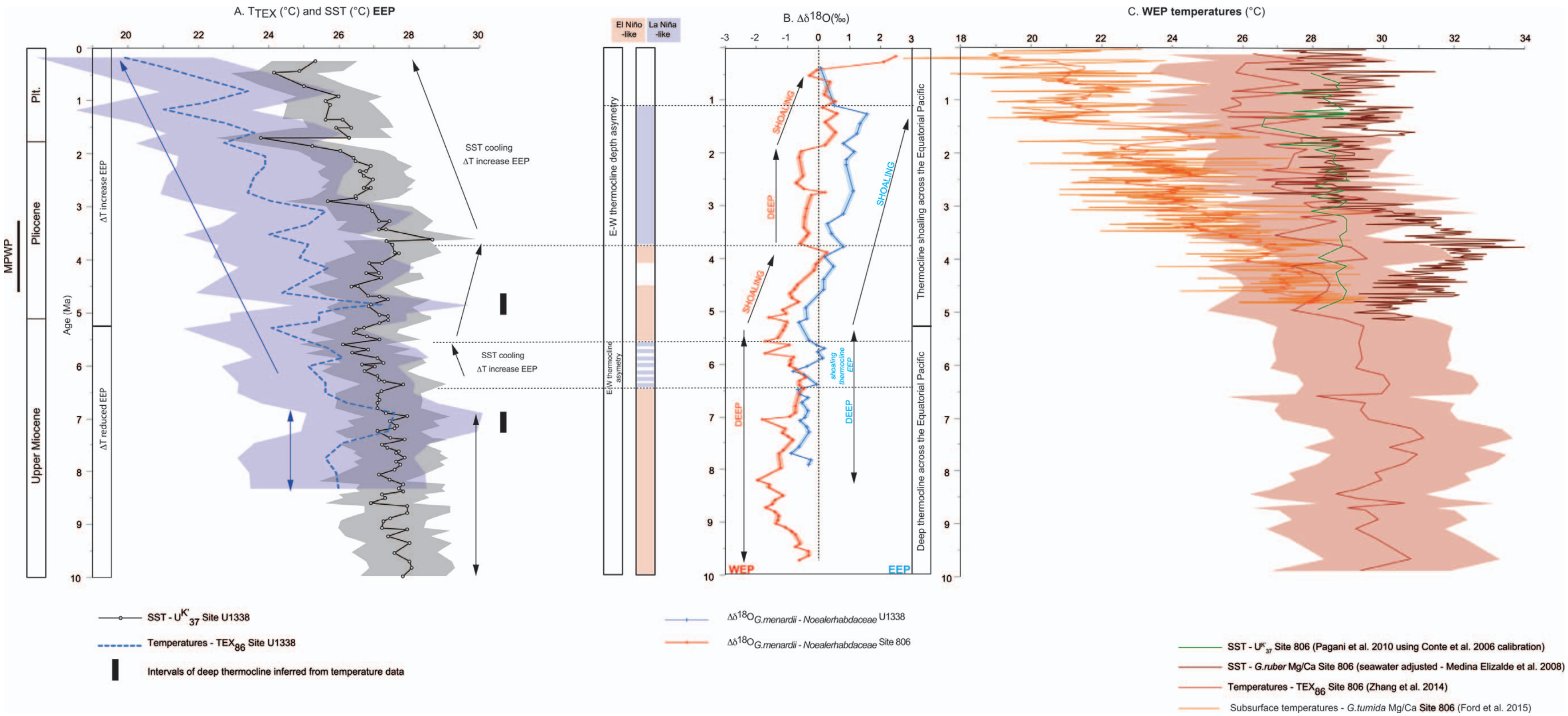

FIG. 4.—**A)** Temperature records at IODP Site U1338 (EEP):$U^{k'}_{37}$-derived SST and TEX_{86}-derived temperatures. The shaded areas represent the error bars of the temperature estimates (light blue: TEX_{86}-derived temperatures and dark blue:$U^{k'}_{37}$-derived SST). The arrows (black and blue) highlight the temperature trends. **B)** Isotopic gradient ($\Delta\delta^{18}O$) between surface and thermocline waters at IODP site U1338 (EEP) and ODP Site 806 (WEP). The evolution of the thermocline depth in the EEP and the WEP over the last 10 Ma according to the $\Delta\delta^{18}O$ is also shown. **C)** Temperature records at ODP Site 806:$U^{k'}_{37}$derived SST (Pagani et al. 2010) in green, TEX_{86}-derived temperatures (Zhang et al. 2014) in red, $Mg/Ca_{G.ruber}$-derived SST (Medina-Elizalde et al. 2008) in brown, and $Mg/Ca_{G.tumida}$-derived temperature (Ford et al. 2015) in orange.

EEP Temperature Reconstructions

Alkenone-derived SSTs ($SST_{U}{}^{K'}{}_{37}$) at Site U1338 are relatively stable and warm ($\sim$ 27°C) between 10 Ma and 6.8 Ma (Fig. 4A). They cool by 1°C between 6.8 Ma and 5.6 Ma, and show a broad warming until 3.7 Ma. From 3.7 Ma onwards, SSTs depict another cooling of about 4°C and superimposed cold episodes of 1 to 2°C amplitude around 2.9 Ma, 1.7 Ma, and 0.5 Ma.

From the late Miocene to the Pleistocene, TEX_{86}-derived temperatures (T_{TEX}) indicate a long-term cooling. Between 8 and 5 Ma, T_{TEX} and the $SST_{U}{}^{K'}{}_{37}$ vary in the same range of values (between 24°C and 27°C; Fig. 4A), although they are slightly cooler. From approx. 4.5 Ma, the two temperature proxies show marked temperature difference. Note that T_{TEX} increase around 7.5 Ma and 4.8 Ma, reaching values close to $SST_{U}{}^{K'}{}_{37}$.

$SST_{U}{}^{K'}{}_{37}$ at Site U1338 are warmer than T_{TEX} by 2 to 3°C on average. Both progressively cool down between 9 Ma and 0.18 Ma but T_{TEX} decreases by 5°C while $SST_{U}{}^{K'}{}_{37}$ cools by only 3°C (Fig. 4A).

DISCUSSION

Surface and Subsurface Water Temperatures in the Equatorial Pacific

Warmer $SST_{U}{}^{K'}{}_{37}$ than T_{TEX}, as observed at Site U1338, is reported in several studies (e.g., Huguet et al. 2007; Lee et al. 2008; Leider et al. 2010; Lopes dos Santos et al. 2010; Rommerskirchen et al. 2011; Seki et al. 2012; Zhang et al. 2014) and explained by different depth habitat or season of production. However, because seasonality is weak at low latitudes, it is unlikely to explain a temperature differences of up to 4°C, at Site U1338. Unlike haptophytes thriving in the photic zone, *Thaumarchaeota*, the sources of the GDGTs, occur throughout the water column (e.g., Karner et al. 2001; Huguet et al. 2007), and the export of GDGTs can be integrated for a larger part of the upper part of the ocean, likely including a part of the thermocline. Wuchter et al. (2005) reported maximum concentrations of GDGTs between 100 and 200 m depth in the Pacific Ocean, coinciding with high ammonium concentrations below the photic zone (Murray et al. 1999; Karner et al. 2001; Wuchter et al. 2005; Huguet et al. 2007; Pearson et al. 2007). GDGT producers can thus preferentially develop in subsurface or deeper waters (Huguet et al. 2007; Kim et al. 2008; Lee et al. 2008; Huguet et al. 2011; Kim et al. 2012). The difference between T_{TEX} and $SST_{U}{}^{K'}{}_{37}$ in the EEP may then account for different production or export depth (Lopes dos Santos et al. 2010; Rommerskirchen et al. 2011; Schouten et al. 2013).

The interpretation of T_{TEX} temperatures across the equatorial Pacific is complicated by both the upwelling in the EEP and the different trophic conditions between the EEP and the WEP that influence the export depth of GDGTs (Seki et al. 2012). Numerous studies indicate that upwelling impacts on the depth of production and export of GDGTs to the sediment (Wuchter et al. 2005; Huguet et al. 2007; Lee et al. 2008; Lopes dos Santos et al. 2010; Seki et al. 2012). In the absence of upwelling, T_{TEX} reflects the surface temperatures (Sinninghe Damsté et al. 2002; Wakeham et al. 2004) whereas under upwelling conditions, T_{TEX} represent thermocline temperatures (Wakeham et al. 2002; Wuchter et al. 2005; Huguet et al. 2007). Furthermore, the nitrate maximum across the modern equatorial Pacific exhibits a clear asymmetry in the depth. Könneke et al. (2005) found that the production of *Thaumarchaeota* occurs in the subsurface nitrate maximum, which thus is deeper in oligotrophic regions such as the WEP (Brzezinski 1988). As a consequence, within the same basin T_{TEX} may reflect surface and subsurface conditions in response to different environmental factors (Hertzberg et al. 2016).

In the EEP, the T_{TEX}-$SST_{U}{}^{K'}{}_{37}$ temperature gradient (ΔT) is proposed to monitor changes of the thermocline depth (Seki et al. 2012) assuming that ΔT is driven by the depth migration of GDGT producers in response to upwelling activity. Therefore, at Site U1338, warming T_{TEX} and reduced ΔT reflect a deep thermocline and surface export of GDGTs, whereas a more pronounced cooling of T_{TEX} compared to $SST_{U}{}^{K'}{}_{37}$ (increased ΔT), reflects a shallow thermocline, upwelling activity, and subsurface export of GDGTs.

In the WEP, the interpretation of T_{TEX}-$SST_{U}{}^{K'}{}_{37}$ is not straightforward either. At Site 806, $SST_{U}{}^{K'}{}_{37}$ calculated from Pagani et al. (2010), are warm and stable, averaging 28 to 28.5°C over the last 5 Myr (Fig. 4C) except for a 2°C sharp cooling at $\sim$ 1.5 Ma. High-resolution Mg/Ca-derived SSTs ($SST_{Mg/Ca}$) corrected from $Mg/Ca_{seawater}$ (Medina-Elizalde et al. 2008) from the same site show markedly warmer conditions in the surface of the WEP especially between 5 and 3.5 Ma, reaching up to 32°C. This difference with the alkenone-derived temperatures can be attributed to (1) the alkenone calibration being less accurate in the warmer temperature range (Conte et al. 2006), thus leading to the underestimation of $SST_{U}{}^{K'}{}_{37}$ (Tierney and Tingley 2018) or (2) the uncertainties on the seawater Mg/Ca correction. However, from 3 Ma onwards, $SST_{U}{}^{K'}{}_{37}$ and $SST_{Mg/Ca}$ temperatures display similar trends and values, except between 1.8 Ma and 1.2 Ma, when they diverge. Since this discrepancy coincides with isotopic changes (Fig. 3) we can reasonably conclude that the difference between the two records during the late Pliocene reflects oceanographic changes. During the early Pliocene, cooler $SST_{U}{}^{K'}{}_{37}$ appear to be linked to a calibration limitation of the proxy at warm temperatures.

Comparison between the T_{TEX} record (Zhang et al. 2014) and subsurface temperatures derived from $Mg/Ca_{G.tumida}$ (Ford et al. 2015) at ODP Site 806, highlights that from 5 to 3.5 Ma both reconstructions agree well within their uncertainties (Fig. 4C). From 3.5 to 2 Ma, T_{TEX} match with $SST_{U}{}^{K'}{}_{37}$ and Mg/Ca-derived SSTs from the surface dweller *G. ruber* ($Mg/Ca_{G.ruber}$ Medina-Elizalde et al. 2008), whereas $Mg/Ca_{G.tumida}$ temperatures are systematically cooler than T_{TEX} (Fig. 4C). After 1.3 Ma, T_{TEX} values are intermediate between $Mg/Ca_{G.ruber}$ and $Mg/Ca_{G.tumida}$ temperatures, while $SST_{U}{}^{K'}{}_{37}$ tend to agree with $Mg/Ca_{G.ruber}$ SSTs. It is likely that in the WEP, the T_{TEX} reflect production in different water depth in response to trophic changes and environmental conditions. We speculate that during the warm early Pliocene and after 1.3 Ma, T_{TEX} reflect subsurface conditions and that during the late Pliocene, the export of GDGTs derived mainly from surface waters. This interpretation nuances the interpretations of Zhang et al. (2014), who considered that T_{TEX} reflect surface temperatures and could be used as an alternative to$U^{k'}_{37}$ under warm conditions.

Changes in the Equatorial Pacific Mean State over the Last 10 Myr

To investigate the evolution of the surface stratification across the Equatorial Pacific, we calculate the oxygen-isotope gradients between *Noelaerhabdaceae* and *G. menardii* ($\Delta\delta^{18}O$) (Fig. 4B) (Nathan and Leckie 2009; Beltran et al. 2014). Note that in doing so, the sea-water $\delta^{18}O$ component is factored out. Higher (lower) $\Delta\delta^{18}O$ values reflect a shallower (deeper) thermocline (Ravelo and Fairbanks 1992; Ravelo and Shackleton 1995; Farell et al. 1995; Nathan and Leckie 2009; Beltran et al. 2014).

Variations in the gradient between T_{TEX} and $SST_{U}{}^{K'}{}_{37}$ also can be used to evaluate changes in the thermocline depth. T_{TEX} and $SST_{U}{}^{K'}{}_{37}$ values similar to those observed between 7.3 Ma and 6.8 Ma, and around 4.8 Ma at IODP Site U1338, indicate a deep thermocline (Fig. 4A). Some intervals are characterized by an increase in ΔT (such as, for example, between 6.8 Ma and 5.3 Ma at IODP Site U1338) associated with a cooling trend of both proxies. These features indicate that GDGTs are produced deeper and that surface waters are concomitantly cooling, which is consistent with upwelling activity.

Based on temperatures and isotopic gradients between surface and subsurface waters from the EEP and WEP, the data reveal a pronounced oceanographic change at ca. 5 Ma with the thermocline progressively rising (Fig. 4A, B).

Late Miocene [9–5.3 Ma] Interval.—During the late Miocene period, east and west $\Delta\delta^{18}O$ are reduced and stable, indicating a deep thermocline across the equatorial Pacific (Fig. 4B). From 10 Ma to 6.3 Ma, data indicate warm SSTs (~ 27 °C) in the EEP (Fig. 4A). This result coincides with the low abundances of upwelling radiolarian species reported between 9 and 7 Ma by Kamikuri et al. (2009). Similar $SST_{U}{}^{K'}{}_{37}$ and T_{TEX} values at U1338 between 7.3 and 6.8 Ma is also consistent with a thick mixed layer in the EEP (Fig. 4A; Seki et al. 2012). In the WEP, Nathan and Leckie (2009) reported a similar decrease in the abundance of surface dwellers in favor of thermocline species, which suggests a deep thermocline. This reduced zonal gradient in SSTs and thermocline tilt across the equatorial Pacific corresponds to El Niño-like conditions, in agreement with earlier findings of Herbert et al. (2016), who indicate an expanded and weak Hadley circulation before 8 Ma.

The long-term late Miocene El Niño-like state was interrupted by a brief interval (6.5–5.3 Ma) during which the thermocline shoaled in the EEP, as shown by the ^{18}O gradient (Fig. 4B). The SST cooling and decrease of surface salinity recorded at Site U1338 (Rousselle et al. 2013), supported by higher abundances of upwelling siliceous species during this interval (Kamikuri et al. 2009), suggest the first establishment of the cold tongue and of upwelling in the EEP. Increasing abundances of surface-dweller species at Site 806 (Nathan and Leckie 2009) (Figs. 3, 4), this interval further supports the idea of a weak and transient La Niña like period. Drury et al. (2018) suggested a cooling of the thermocline waters related to the global late Miocene cooling (Fedorov et al. 2006; Drury et al. 2017). Although the data do not rule out this hypothesis, the T_{TEX} cooling is supportive of a change in depth of GDGT production or export in response to the onset of the EEP upwelling.

Plio-Pleistocene (from 5.3 Ma) Interval.—The oxygen-isotope and temperature data indicate a long-term gradual thermocline shoaling and sea-surface cooling in the EEP (Fig. 4A, B) throughout this interval. In the WEP, the thermocline shoaled between 5.3 and 4 Ma, returning to a deep position between 4 and 1.8 Ma and shoaling again after 1.8 Ma. This interval is characterized by the initiation of a progressive asymmetry in the thermocline depth across the equatorial Pacific.

After 5.3 Ma, SSTs at IODP Site U1338 were warm (~ 27 °C), in agreement with a deep thermocline until 4.5 Ma (Fig. 4A). This result is supported by a rapid increase of T_{TEX} at U1338. Moreover, abundances of upwelling radiolarian species decreased again in the EEP (Kamikuri et al. 2009). In the WEP, the proto-warm pool period ended (Nathan and Leckie 2009). This interval coincides with the Messinian salinity crisis (Hilgen et al. 2007), during which the isolation of the Mediterranean Sea would have triggered a reduction of the North Atlantic Deep Water formation (NADW) at ~ 6 Ma because of changing water density of the North Atlantic waters (Pérez-Asensio et al. 2012). According to model simulations, this process would result in a deepening of the thermocline in the equator and El Niño-like conditions (Rühlemann et al. 2004; Timmermann et al. 2005; Barreiro et al. 2008), thus providing a possible explanation to the results herein.

Numerous studies have focused on the magnitude of Pliocene equatorial Pacific warmth (4.5 – 3.5 Ma) and the factors responsible for it (e.g., Raymo et al. 1996; Haywood and Valdes 2004; Ravelo et al. 2004; Barreiro et al. 2008; Rickaby and Halloran 2005; Brierley et al. 2009; Scroxton et al. 2011; Ford et al. 2015). It is accepted that during the mid-Piacenzian Warm Period, persistent El-Niño like conditions prevailed. This interval, also known as the El Padre mean state (Ford et al. 2015), is characterized by a deep and warm thermocline and warm surface conditions across the equatorial Pacific.

The low-resolution record presented here suggests a brief interval centered around 4 Ma when the thermocline deepened in the east and shoals in the west. SSTs in the EEP reach 30°C and around 32°C in the WEP (Fig. 4A, C, $Mg/Ca_{G.ruber}$ SSTs; Medina-Elizalde et al. 2008). From 3.5 Ma, a pronounced zonal gradient of the thermocline depth and of the SSTs developed across the Pacific. The SST cooling trend and shoaling of the thermocline identified in the EEP coincides with the permanent establishment of the cold tongue (Groeneveld et al. 2006; Dekens et al. 2007; Steph et al. 2010; Rousselle et al. 2013). This result is in agreement with Chaisson and Ravelo (2000) and Kamikuri et al. (2009), who report higher abundances of subsurface-dweller foraminifera and radiolarian upwelling species in the EEP at that time. Simultaneous with the changes in the EEP, the warm pool became established and the thermocline deepened in the WEP, as suggested by warmer surface waters and reduced ΔT (Fig. 4C, Wara et al. 2005; Medina-Elizalde et al. 2008) and planktonic foraminifera abundances (Cannariato and Ravelo 1997; Chaisson and Ravelo 2000; Li et al. 2006). This La Niña-like pattern is consistent with earlier studies (Rickaby and Halloran 2005; Kamikuri et al. 2009; Steph et al. 2010; Ford et al. 2012 and Rousselle et al. 2013) in favor of an active equatorial upwelling and a strong Walker cell.

Between 1.8 and 1.3 Ma, data indicate that the thermocline tilt and the SST gradient across the Pacific were reinforced (Fig. 4). This result is in agreement with the setting of the modern cold tongue identified by Martinez-Garcia et al. (2011).

Evolution of the Pacific Mean State in a Regional and Global Context

Prior research has attributed changes in the thermocline tilt to local tectonic events such as the opening and closing of the Panama and Indonesian oceanic gateways (e.g., LaRiviere et al. 2012), and changes in sea-surface-temperature zonal gradients to global climate perturbations or changes in regional wind patterns and strength (Hovan 1995; Ford et al. 2012).

However, there is still a strong debate about the timing of the closure of these oceanic gateways and their role in controlling the equatorial Pacific mean climate state. Montes et al. (2012, 2015), Osborne et al. (2014), and Sepulchre et al. (2014) suggested that the Central American Seaway was restricted by 10–11 Ma, which contradicts the commonly accepted late Pliocene timing of its closure (Keigwin 1982; Duque-Caro 1990; Haug and Tiedemann 1998; Haug et al. 2001). On the other hand, Molnar and Cronin (2015) showed a marked restriction of the Indonesian Seaway from 5 Ma. This interpretation implies that the changes of the equatorial Pacific mean state during the Miocene would have been controlled mainly by global climate changes.

The brief La Niña-like interval between 6.5 and 5.3 Ma may be attributable to the combination of the restricted flow through the Central American Seaway (Keigwin 1982; Keller et al. 1989) and the 25 m sea-level drop at ~ 6.5 Ma (Haq et al. 1987; Hardenbol et al. 1998; Haq and Schutter 2008) due to the expansion of ice sheets in Greenland (Larsen et al. 1994), Alaska (Bradshaw et al. 2012) and Antarctica (Billups 2002; Williams et al. 2010), and the 2 Myr-long Northern Hemisphere glaciation (Larsen et al. 1994). This global cooling is thought to have contributed to the reinforcement of the equatorial upwelling and EUC.

Data from sediments younger than ~ 5 Ma indicate an important change in the equatorial Pacific mean state with the dominance of La Niña-like intervals. The onset of this long-term state coincides with a drastic restriction of the Indonesian Seaway (Srinivasan and Sinha 1998; Molnar and Cronin 2015), and changes in the global climate. The Indonesian Seaway restriction is thought to have contributed to the cooling of the eastern tropical Pacific over the last 5 Myr through the strengthening of the Walker circulation, leading to the increase in the Pacific zonal temperature gradient (Figs. 3, 4).

The La Niña-like event between 1.8 and 1.3 Ma coincides with pronounced ice growth in Antarctica (McKay et al. 2012) and the development of the northern-hemisphere ice sheets. The gradual increase of the pole-to-equator temperature gradient is thought to have reinforced the Walker cell, and affected the low-latitude zonal gradient (Molnar and Cane 2002; McKay et al. 2012). Furthermore, modeling experiments show a positive feedback of the Pliocene low-latitude cooling on the global cooling (Fedorov et al. 2006). The shoaling of the thermocline increased the climate sensitivity of this area by strengthening the temperature gradient through the tropics and subsequently the Walker and Hadley cells (Brierley et al. 2009; Brierley and Fedorov 2010). These processes led to the final setting of upwelling areas (Philander and Fedorov 2003; Dekens et al. 2007; Brierley et al. 2009; Brierley and Fedorov 2010).

CONCLUSIONS

This study demonstrates the complexity of reconstructing the evolution of the equatorial Pacific mean climate state and oceanographic features and the need of a multi-proxy approach to get a comprehensive understanding of the mechanisms at play over the past 10 Myr. Combined isotopic zonal gradients between the surface (*Noelaerhabdaceae*) and subsurface (*G. menardii*) waters from the east and west equatorial Pacific reveals important steps towards the establishment of what is known today as El Niño–Southern Oscillation. The record suggests a general shoaling of the thermocline along the equator since the late Miocene. The data show the appearance of the cold tongue at $\sim$ 6.8 Ma before its proper establishment around 4.4 to 3.6 Ma (Chaisson 1995; Cannariato and Ravelo 1997; Chaisson and Ravelo 2000; Molnar and Cane 2002; Ravelo et al. 2004, 2006; Sato et al. 2008; Steph et al. 2010; Rousselle et al. 2013) and its modern configuration $\sim$ 1.8 Ma. This result is in agreement with the findings of LaRivière et al. (2012) and Zhang et al. (2014), who suggested progressive shoaling of the thermocline over the last 13 Myr.

The data indicate two critical transitions at about 5.3 Ma, when the thermocline globally started shoaling across the equatorial Pacific and around 3.8 Ma from an El-Niño-like-dominated mean state during the late Miocene to a La-Niña-like-dominated state during the Plio-Pleistocene. These transitions coincide with marked regional and global changes. Locally, the restriction of the Indonesian Seaway and subsequent intensification of the Walker circulation increased the Pacific zonal temperature gradient over the last 5 Myr. From a global point of view, the growth of ice sheets in the northern hemisphere and in Antarctica most likely affected the Walker cell and the low-latitude zonal gradient.

SUPPLEMENTAL MATERIAL

Two supplemental files are available from JSR's Data Archive: https://www.sepm.org/pages.aspx?pageid=229.

ACKNOWLEDGMENTS

We thank the European Consortium for Ocean Research Drilling (ECORD) for the ECORD Grant. We are also grateful to Anchelique Mets and Jort Ossebaar for support with the TEX_{86} measurements. We finally want to thank Fabrice Minoletti for developing the separation technique necessary to perform the isotopic measurements on *Noelaerhabdaceae* calcite. We also thank the Ocean and International Ocean Drilling Program (ODP and IODP) for providing samples from Sites 806 and U1338. SS and AS were supported by the Netherlands Earth System Science Center funded by the Dutch Ministry Science and Education (OCW). MAS was supported by CNRS (Centre National de la Recherche Scientifique) for salary.

REFERENCES

Backman, J., Baldauf, J.G., Ciummelli, M., and Raffi, I., 2016, Data report: a revised biomagnetostratigraphic age model for Site U1338, IODP Expedition 320/321: Proceedings of the Integrated Ocean Drilling Program, 320/321. DOI: 10.2204/iodp.proc.320321.219.2016

Barreiro, M., Philander, G., Pacanowski, R., and Fedorov, A., 2005, Simulations of warm tropical conditions with application to middle Pliocene atmospheres: Climate Dynamics, v. 26, p. 349–365.

Barreiro, M., Fedorov, A., Pacanowski, R., and Philander, S.G., 2008, Abrupt climate changes: how freshening of the Northern Atlantic affects the thermohaline and wind-driven oceanic circulations: Annual Review of Earth and Planetary Sciences, v. 36, p. 33–58.

Beltran, C., Rousselle, G., Backman, J., Wade, B.S., and Sicre, M.A., 2014, Paleoenvironmental trigger for the development of bloom forming calcareous nannofossils: an example from the Late Miocene Eastern Equatorial Pacific: Palaeoceanography, v. 29, p. 210–222.

Billups, K., 2002, Late Miocene through early Pliocene deep water circulation and climate change viewed from the sub-Antarctic South Atlantic: Palaeogeography, Palaeoclimatology, Palaeoecology, v. 185, p. 287–307.

Boccaletti, G., Pacanowski, R.C., Philander, S.G.H., and Fedorov, A.V., 2004, The thermal structure of the upper ocean: Journal of Physical Oceanography, v. 34, p. 888–902

Bradshaw, C.D., Lunt, D.J., Flecker, R., Salzmann, U., Pound, M.J., Haywood, A.M., and Eronen, J.T., 2012, The relative roles of CO_2 and palaeogeography in determining late Miocene climate: Results from a terrestrial model-data comparison: Climate of the Past, v. 8, p. 1257–1285.

Brassell, S.C., Eglinton, G., Marlowe, I.T., Pflaumann, U., and Sarnthein, M., 1986, Molecular stratigraphy: a new tool for climatic assessment: Nature, v. 320, p. 129–133.

Brierley, C.M., and Fedorov, A.V., 2010, Relative importance of meridional and zonal sea surface temperature gradients for the onset of the ice ages and Pliocene–Pleistocene climate evolution: Paleoceanography, v. 25, PA2214. DOI:10.1029/2009PA001809

Brierley, C., Fedorov, A.V., Liu, Z., Herbert, T.D., Lawrence, K.T., and LaRivière, J.P., 2009, Greatly expanded tropical warm pool and weakened Hadley circulation in the early Pliocene: Science, v. 323, p. 1714–1718.

Brzezinski, M.A., 1988, Vertical distribution of ammonium in stratified oligotrophic waters: Limnology and Oceanography, v. 33, p. 1176–1182.

Cane, M.A., 1998, A role for the tropical Pacific: Science, v. 282, p. 59–61. DOI: 10.1126/science.282.5386.59

Cannariato, K.G., and Ravelo, A.C., 1997, Pliocene–Pleistocene evolution of eastern tropical Pacific surface water circulation and thermocline depth: Paleoceanography, v. 12, p. 805–820.

Chaisson W.P., 1995, Planctonic foraminiferal assemblages and paleoceanographic change in the trans-tropical Pacific Ocean: a comparison of west (leg 130) and east (leg 138), latest Miocene to Pleistocene: Proceedings of the Ocean Drilling Program, Scientific Results, v. 138, p. 555–581.

Chaisson, W.P., and Leckie, R.M., 1993, High-resolution Neogene planktonic foraminifer biostratigraphy of Site 806, Ontong Java Plateau (western equatorial Pacific), *in* Berger, W.H., Kroenke, L.W., Mayer, L.A., et al., eds., Proceedings of Ocean Drilling Program, Scientific Results, v. 130, p. 137–178.

Chaisson, W.P., and Ravelo, A.C., 2000, Pliocene development of the east–west hydrographic gradient in the equatorial Pacific: Paleoceanography, v. 15, p. 497–505.

Conte, M.H., Sicre, M.-A., Rühlemann, C., Weber, J.C., Schulte, S., Schulz-Bull, D., and Blanz, T., 2006, Global calibration of the alkenone unsaturation index ($U^{K'}_{37}$) with surface water production temperature and a comparison of the core top integrated production temperatures recorded by $U^{K'}_{37}$ with overlying sea surface temperatures: Geochemistry, Geophysics, Geosystems, v. 7, p. 1–22.

Dekens, P.S., Ravelo, A.C., and McCarthy, M.D., 2007, Warm upwelling regions in the Pliocene warm period: Paleoceanography, v. 22, p. 1–12.

Dekens, P.S., Ravelo, A.C., McCarthy, M.D., and Edwards, C.A., 2008, A 5 million year comparison of Mg/Ca and alkenone paleothermometers: Geochemistry, Geophysics, Geosystems, v. 9. DOI:10.1029/2007GC001931

Drury, A.J., Westerhold, T., Frederichs, T., Tian, J., Wilkens, R., Channell, J.E.T., Evans, H., John, C.M., Lyle, M., and Röhl, U., 2017, Late Miocene climate and time scale reconciliation: accurate orbital calibration from a deep-sea perspective: Earth and Planetary Science Letters, v. 475, p. 254–266.

Drury, A.J., Geoff, L., Gray, W.R., Lyle, M., Westerhold, T., Shevenell, A., and John, C., 2018, Deciphering the State of the Late Miocene to Early Pliocene Equatorial Pacific: Paleoceanography and Paleoclimatology, v. 33, DOI:10.1002/2017PA003245.

Duque-Caro, H., 1990, Neogene stratigraphy, paleoceanography and paleobiogeography in northwest South America and the evolution of the Panama Seaway: Palaeogeography, Palaeoclimatology, Palaeoecology, v. 77, p. 203–234.

Farell, J.W., Raffi, I., Janecek, T.R., Murray, D.W., Levitan, M., Dadey, K.A., Emeis, K., Lyle, M., Flores, J.-A., and Hovan, S., 1995, Late Neogene sedimentation patterns in the eastern equatorial Pacific Ocean: Proceedings of the Ocean Drilling Program, Scientific Results, v. 138, p. 717–756.

Fedorov, A.V., Dekens, P.S., McCarthy, M., Ravelo, A.C., DeMenocal, P.B., Barreiro, M., Pacanowki, R.C., and Philander, S.G., 2006, The Pliocene paradox (mechanisms for a permanent El Niño): Science, v. 312, p. 1485–1489.

Fedorov, A.V., Brierley, C.M., Lawrence, K.T., Liu, Z., Dekens, P.S., and Ravelo, A., 2013, Patterns and mechanisms of early Pliocene warmth: Nature, v. 496, p. 43–49. DOI:10.1038/nature12003

Ford, H.L., Ravelo, A.C., and Hovan, S., 2012, A deep Eastern Equatorial Pacific thermocline during the early Pliocene warm period: Earth and Planetary Science Letters, v. 355–356, p. 152–161.

Ford, H.L., Ravelo, A.C., Dekens, P.S., LaRivière, J.P., and Wara, M.W., 2015, The evolution of the equatorial thermocline and the early Pliocene El Padre mean state: Geophysical Research Letters, v. 42, p. 4878–4887. DOI:10.1002/ 2015GL064215

Groeneveld, J., Steph, S., Tiedemann, R., Garbe, D., Nürnberg, D., and Sturn, A., 2006, Pliocene mixed-layer oceanography for site 1241, using combined Mg/Ca and $\delta^{18}O$ analyses of *Globigerinoides sacculifer*: Proceedings of the Ocean Drilling Program, Scientific Results, v. 202, p. 1–27.

HAQ, B.U., AND SCHUTTER, S.R., 2008, A chronology of Paleozoic sea-level changes: Science, v. 322, p. 64–68.

HAQ, B.U., HARDENBOL, J., AND VAIL, P.R., 1987, Chronology of fluctuating sea levels since the Triassic (250 million years ago to present): Science, v. 235, p. 1156–1167.

HARDENBOL, J., THIERRY, J., FARLEY, M.B., JACQUIN, T., DE GRACIANSKY, P.C., AND VAIL, P., 1998, Mesozoic and Cenozoic sequence chronostratigraphic framework of European basins, *in* De Graciansky, P.-C., Hardenbol, J., Jacquin, T., Vail, P.R., and Farley, M.B., eds., Mesozoic and Cenozoic Sequence Stratigraphy of European Basins: SEPM, Special Publication 60, p. 3–13.

HAUG, G.H., AND TIEDEMANN, R., 1998, Effect of the formation of the Isthmus of Panama on Atlantic Ocean thermohaline circulation: Nature, v. 393, p. 673–676.

HAUG, G.H., TIEDEMANN, R., ZAHN, R., AND RAVELO, A.C., 2001, Role of Panama uplift on oceanic freshwater balance: Geology, v. 29, p. 207–210.

HAYWOOD, A.M., AND VALDES, P.J., 2004, Modelling middle Pliocene warmth: contribution of atmosphere, oceans and cryosphere: Earth and Planetary Science Letters, v. 218, p. 363–377.

HERBERT, T.D., LAWRENCE, K.T., TZANOVA, A., PETERSON, L.C., CABALLERO-GILL, R., AND KELLY, C.S., 2016, Late Miocene global cooling and the rise of modern ecosystems: Nature Geoscience, v. 9, p. 843–847. DOI:10.1038/NGEO2813

HERTZBERG, J.E., SCHMIDT M.W., BIANCHI, T.S., SMITH, R.W., SHIELDS, M.R., AND MARCANTONIO, F., 2016, Comparison of eastern tropical Pacific TEX_{86} and *Globigerinoides ruber* Mg/Ca derived sea surface temperatures: insights from the Holocene and Last Glacial Maximum: Earth and Planetary Science Letters, v. 434, p. 320–332.

HILGEN, F., KUIPER, K., KRIJGSMAN, W., SNEL, E., AND VAN DER LAAN, E., 2007, Astronomical tuning as the basis for high resolution chronostratigraphy: the intricate history of the Messinian Salinity Crisis: Stratigraphy, v. 4, p. 231–238.

HOVAN, S.A., 1995, Late Cenozoic atmospheric circulation intensity and climatic history recorded by eolian deposition in the eastern equatorial Pacific Ocean, Leg 138: Proceedings of the Ocean Drilling Program, Scientific Results, v. 138, p. 615–625.

HUGUET, C., SCHIMMELMANN, A., THUNELL, R., LOURENS, L.J., SINNINGHE DAMSTÉ, J., AND SCHOUTEN, S., 2007, A study of the TEX_{86} paleothermometer in the water column and sediments of the Santa Barbara Basin, California: Paleoceanography, v. 22, p. 9.

HUGUET, C., MARTRAT, B., GRIMALT, J.O., SINNINGHE DAMSTÉ, J.S., AND SCHOUTEN, S., 2011, Coherent millennial scale patterns in$U^{k'}_{37}$ and TEX^{H}_{86} temperature records during the penultimate interglacial-to-glacial cycle in the western Mediterranean: Paleoceanography, v. 26, p. 10.

KAMIKURI, S., MOTOYAMA, I., NISHI, H., AND IWAI, M., 2009, Evolution of Eastern Warm Pool and upwelling processes since the middle Miocene based on analysis of radiolarian assemblages: response to Indonesian and Central American Seaways: Palaogeography, Palaeoclimatology, Palaeoecology, v. 280, p. 469–479.

KARNER, M.B., DELONG, E.F., AND KARL, D.M., 2001, Archaeal dominance in the mesopelagic zone of the Pacific Ocean: Nature, v. 409, p. 507–510.

KEIGWIN, L.D., 1982, Isotope paleoceanography of the Caribbean and east Pacific: role of Panama uplift in late Neogene time: Science, v. 217, p. 350–353.

KELLER, G., ZENKER, C.E., AND STONE, S.M., 1989, Late Neogene history of the Pacific–Caribbean gateway: Journal of South American Earth Sciences, v. 2, p. 73–108.

KIM, J.H., SCHOUTEN, S., HOPMANS, E.C., DONNER, B., AND SINNINGHE DAMSTÉ, J.S., 2008, Global sediment core-top calibration of the TEX_{86} paleothermometer in the ocean: Geochimica et Cosmochimica Acta, v. 72, p. 1154–1173.

KIM, J.H., VAN DER MEER, J., SCHOUTEN, S., HELMKE, P., WILLMOTT, V., SANGIORGI, F., KOÇ, N., HOPMANS, E.C., AND SINNINGHE DAMSTÉ, J.S., 2010, New indices and calibrations derived from the distribution of crenarchaeal isoprenoid tetraether lipids: implications for past sea surface temperature reconstructions: Geochimica et Cosmochimica Acta, v. 74, p. 4639–4654.

KIM, J.H., ROMERO, O.E., LOHMANN, G., DONNER, B., LAEPPLE, T., HAAM, E., AND SINNINGHE DAMSTÉ, J.S., 2012, Pronounced subsurface cooling of North Atlantic waters off Northwest Africa during Dansgaard–Oeschger interstadials: Earth and Planetary Science Letters, v. 339–340, p. 95–102.

KÖNNEKE, M., BERNHARD, A.E., DE LA TORRE, J.R., WALKER, C.B., WATERBURY, J.B., AND STAHL, D.A., 2005, Isolation of an autotrophic ammonia-oxidizing marine Archaeon: Nature, v. 437, p. 543–546.

KOUTAVAS, A., DEMENOCAL, G., OLIVE, C., AND LYNCH-STIEGLITZ, J., 2006, Mid-Holocene El Niño–Southern Oscillation (ENSO) attenuation revealed by individual foraminifera in eastern tropical Pacific sediments: Geology, v. 34, p. 993–996.

KROENKE, L.W., BERGER, W.H., AND JANECEK, T.R., 1991, Site 806: Proceedings of the Ocean Drilling Program, Initial Reports, v. 130, p. 291–367.

LARIVIÈRE, J.P., RAVELO, A.C., CRIMMINS, A., DEKENS, P.S., FORD, H.L., LYLE, M., AND WARA, M.W., 2012, Late Miocene decoupling of oceanic warmth and atmospheric carbon dioxide forcing: Nature, v. 486, p. 97–100.

LARSEN, H.C., SAUNDERS, A.D., CLIFT, P.D., BEGET, J., WEI, W., AND SPEZZAFERRI, S., 1994, Seven million years of glaciation in Greenland: Science, v. 264, p. 952–955.

LEE, K.E., KIM, J.H., WILKE, I., HELMKE, P., AND SCHOUTEN, S., 2008, A study of the alkenone TEX_{86} and planktonic foraminifera in the Benguela Upwelling System: implications for past sea surface temperatures estimates: Geochemistry, Geophysics, Geosystems, v. 9, p. 19.

LEIDER, A., HINRICHS, K.U., MOLLENHAUER, G., AND VERSTEEGH, G.J.M., 2010, Core-top calibration of the lipid-based$U^{k'}_{37}$ and TEX_{86} temperature proxies on the southern Italian shelf (SW Adriatic Sea, Gulf of Taranto): Earth and Planetary Science Letters, v. 300, p. 112–124.

LI, Q., LI, B., ZHONG, G., MCGOWRAN, B., ZHOU, Z., WANG, J., AND WANG, P., 2006, Late Miocene development of the western Pacific warm pool: planktonic foraminifer and oxygen isotopic evidence: Palaeogeography, Palaeoclimatology, Palaeoecology, v. 237, p. 465–482.

LOPES DOS SANTOS, R.A., PRANGE, M., CASTAÑEDA, I.S., SCHEFUß, E., MULITZA, S., SCHULZ, M., NIEDERMEYER, E.M., SINNINGHE DAMSTÉ, J.S., AND SCHOUTEN, S., 2010, Glacial–interglacial variability in Atlantic meridional overturning circulation and thermocline adjustments in the tropical North Atlantic: Earth and Planetary Science Letters, v. 300, p. 407–414.

MARTIN, R.E., 1999, Taphonomy and temporal resolution of foraminiferal assemblages, *in* Sen Gupta, B.K., ed., Modern Foraminifera: Kluwer Academic Publishers, 371 p.

MARTINEZ-GARCIA, A., ROSELL-MELE, A., JACCARD, S.L., GEIBERT, W., SIGMAN, D.M., AND HAUG, G.H., 2011, Southern Ocean dust: climate coupling over the past four million years: Nature, v. 476, p. 312–315. DOI:10.1038/nature10310

MCKAY, R., NAISH, T., CARTER, L., RIESSELMAN, C., DUNBAR, R., SJUNNESKOG, C., WINTER, D., SANGIORGI, F., WARREN, C., PAGANI, M., SCHOUTEN, S., WILLMOTT, V., LEVY, R., DECONTO, R., AND POWELL, R.D., 2012, Antarctic and Southern Ocean influences on late Pliocene global cooling: National Academy of Sciences (U.S.A.), Proceedings, v. 109, p. 6423–6428.

MCPHADEN, M.J., ZEBIAK, S.E., AND GLANTZ, M.H., 2006, ENSO as an integrating concept in Earth science: Science, v. 314, p. 1740–1745.

MEDINA-ELIZALDE, M., AND LEA, D.W., 2010, Late Pliocene equatorial Pacific: Paleoceanography, v. 25, PA2208. DOI:10.1029/2009PA001780

MEDINA-ELIZALDE, M., LEA, D.W., AND FANTLE, M.S., 2008, Implications of seawater Mg/Ca variability for Plio-Pleistocene tropical climate reconstruction: Earth and Planetary Science Letters, v. 269, p. 584–594.

MINOLETTI, F., HERMOSO, M., AND GRESSIER, V., 2009, Separation of sedimentary micron-size particles for palaeoceanography and calcareous nannoplankton biogeochemistry: Nature Protocols, v. 4, p. 14–24.

MOLNAR, P., AND CANE, M.A., 2002, El Niño's tropical climate and teleconnections as a blueprint for pre-Ice Age climate: Paleoceanography, v. 172, p. 1–13.

MOLNAR, P., AND CRONIN, T.W., 2015, Growth of the maritime continent and its possible contribution to recurring Ice Ages: Paleoceanography, v. 30, p. 196–225.

MONTES, C., CARDONA, A., MCFADDEN, R., MORÓN, S., SILVA, J.C., RESTREPO-MORENO, S., RAMIREZ, D., HOYOS, N., WILSON, J. FARRIS, D., BAYONA, G., JARAMILLO, C., VALENCIA, V., BRYAN, J., AND FLORES, J.A., 2012, Evidence for middle Eocene and younger land emergence in Central Panama: implications for Isthmus closure: Geological Society of America, Bulletin, v. 124, p. 780–799.

MONTES, C., CARDONA, A., JARAMILLO, C., PARDO, A., SILVA, J.C., VALENCIA, V., AYALA, C., PÉREZ-ANGEL, L.C., RODRIGUEZ-PARRA, L.A., RAMIREZ, V., AND NIÑO, H., 2015, Middle Miocene closure of the Central American Seaway: Science, v. 348, p. 226–229. DOI:10.1126/science.aaa2815

MUDELSEE, M., AND RAYMO, M.E., 2005, Slow dynamics of the Northern Hemisphere glaciation: Paleoceanography, v. 20, PA4022. DOI:10.1029/2005PA001153

MURRAY, A.E., BLAKIS, A., MASSANA, R., STRAWZEWSKI, S., PASSOW, U., ALLDREDGE, A., AND DELONG, E.F., 1999, A time series assessment of planktonic archaeal variability in the Santa Barbara Channel: Aquatic Microbial Ecology, v. 20, p. 129–145.

NATHAN, S.A., AND LECKIE, R.M., 2009, Early history of the Western Pacific Warm Pool during the middle to late Miocene ($\sim$13.2–5.8 Ma): role of sea-level change and implications for equatorial circulation: Palaeogeography, Palaeoclimatology, Palaeoecology, v. 274, p. 140–159.

NEELIN, J.D., BATTISTI, D.S., HIRST, A.C., JIN, F.-F., WAKATA, Y., YAMAGATA, T., AND ZEBIAK, S.E., 1998, ENSO Theory: Journal of Geophysics Research, v. 103, p. 14,261–14,290.

OSBORNE, A.H., NEWKIRK, D.R., GROENEVELD, J., MARTIN, E.E., TIEDEMANN, R., AND FRANK, M., 2014, The seawater neodymium and lead isotope record of the final stages of Central American Seaway closure: Paleoceanography, v. 29, p. 715–729. DOI:10.1002/2014PA002676

PAGANI, M., LIU, Z., LARIVIERE, J., AND RAVELO, A.C., 2010, High Earth-system climate sensitivity determined from Pliocene carbon dioxide concentrations: Nature Geoscience, v. 3, p. 27–30.

PÄLIKE, H., LYLE, M., NISHI, H., RAFFI, I., GAMAGE, K., KLAUS, A., AND THE EXPEDITION 320/321 SCIENTISTS, 2010, Site 1338: International Ocean Drilling Program, 320/321, Expedition Reports, Proceedings, v. 321, 141 p.

PÄLIKE, H., LYLE, M.W., NISHI, H., AND RAFFI, I., ET AL., 2012, A Cenozoic record of the equatorial Pacific carbonate compensation depth: Nature, v. 488, p. 609–614. DOI:10.1038/nature11360

PEARSON, P.N., VAN DONGEN, B.E., NICHOLAS, C.J., PANCOST, R.D., SCHOUTEN, S., SINGANO, J.M., AND WADE, B.S., 2007, Stable warm tropical climate through the Eocene epoch: Geology, v. 35, p. 211–214.

PÉREZ-ASENSIO, J.N., SCHMIEDL, G., AGUIRRE, J., AND CIVIS, J., 2012, Impact of restriction of the Atlantic–Mediterranean gateway on the Mediterranean Outflow Water and eastern Atlantic circulation during the Messinian: Paleoceanography, v. 27, PA3222. DOI:10.1029/2012PA002309

PHILANDER, S., AND FEDOROV, A., 2003, Role of tropics in changing the response to Milankovich forcing some three million years ago: Paleoceanography, v. 18. DOI:10.1029/2002PA000837

PISIAS, N.G., MAYER AND MIX, A.C., 1995, Paleoceanography of the eastern equatorial Pacific during the Neogene: synthesis of Leg 138 drilling results, *in* Pisias, N.G., Mayer, L.A., Janecek, T.R., Palmer-Julson, A., and van Andel, T.H., eds., Proceedings of the Ocean Drilling Program, Scientific Results, v. 138, p. 5–21.

Prahl, F.G., Muehlhausen, L.A., and Zahnle, D.L., 1988, Further evaluation of long-chain alkenones as indicators of paleoceanographic conditions: Geochimica et Cosmochimica Acta, v. 52, p. 2303–2310.

Ravelo, A.C., and Fairbanks, R.G., 1992, Oxygen isotopic composition of multiple species of planktonic foraminifera: recorders of the modern photic zone temperature gradient: Paleoceanography, v. 7, p. 815–831.

Ravelo, A.C., and Shackleton, N.J., 1995, Evidence for surface-water circulation changes at Site 851 in the eastern tropical Pacific Ocean: Ocean Drilling Program, Scientific Results, Proceedings, v. 138, p. 503–514.

Ravelo, A.C., Andreasen, D., Lyle, M., Olivarez, L., and Wara, M.W., 2004, Regional climate shifts caused by gradual global cooling in the Pliocene Epoch: Nature, v. 429, p. 263–267.

Ravelo, A.C., Dekens, P.S., and McCarthy, M., 2006, Evidence for El Niño-like conditions during the Pliocene: GSA Today, v. 16, p. 4–11.

Raymo, M.E., Grant, B., Horowitz, M., and Rau, G.H., 1996, Mid-Pliocene warmth: stronger greenhouse and stronger conveyor: Marine Micropaleontology, v. 27, p. 313–326.

Rickaby, R.E.M., and Halloran, P., 2005, Cool La Niña the warmth of the Pliocene: Science, v. 307, p. 1948–1952.

Rommerskirchen, F., Condon, T., Mollenhauer, G., Dupont, L., and Schefuss, E., 2011, Miocene to Pliocene development of surface and subsurface temperatures in the Benguela Current system: Paleoceanography, v. 26, 15 p.

Roth, P.H., 1986, Mesozoic paleoceanography of the North Atlantic and Tethys oceans, North Atlantic: Paleoceanography, v. 21, p. 299–320.

Rousselle, G., Beltran, C., Sicre, M.-A., Raffi, I., and De Rafélis, M., 2013, Sea-surface condition changes in the equatorial Pacific during the Mio-Pliocene as inferred from coccolith geochemistry: Earth and Planetary Science Letters, v. 361, p. 412–421.

Rühlemann, C., Mulitza, S., Lohmann, G., Paul, A., Prange, M., and Wefer, G., 2004, Intermediate depth warming in the tropical Atlantic related to weakened thermohaline circulation: combining paleoclimate data and modelling results for the last deglaciation: Paleoceanography, v. 19, 10 p.

Sato, K., Oda, M., Chiyonobu, S., Kimoto, K., Domitsu, H., and Ingle, J.C., 2008, Establishment of the western Pacific warm pool during the Pliocene: evidence from planktic foraminifera, oxygen isotopes, and Mg/Ca ratios: Palaeogeography, Palaeoclimatology, Palaeoecology, v. 265, p. 140–147.

Schneider, B., and Schmittner, A., 2006, Simulating the impact of the Panamanian seaway closure on ocean circulation, marine productivity and nutrient cycling: Earth and Planetary Science Letters, v. 246, p. 367–380.

Schouten, S., Hopmans, E.C., Schefuss, E., and Sinninghe Damsté, J.S., 2002, Distributional variations in marine crenarchaeotal membrane lipids: a new tool for reconstructing ancient sea water temperatures?: Earth and Planetary Science Letters, v. 204, p. 265–274.

Schouten, S., Huguet, C., Hopmans, E.C., Kienhuis, M.V.M., and Sinninghe Damsté, J.S., 2007, Improved analytical methodology and constraints on analysis of the TEX_{86} paleothermometer by high performance liquid chromatography/atmospheric pressure chemical ionization-mass spectrometry: Analytical Chemistry, v. 79, p. 2940–2944.

Schouten, S., Hopmans, E.C., and Sinninghe Damsté, J.S., 2013, The organic geochemistry of glycerol dialkyl glycerol tetraether lipids: a review: Organic Geochemistry, v. 54, p. 19–61.

Scroxton, N., Bonham, S.G., Rickaby, R.E.M., Lawrence, S.H.F., Hermoso, M., and Haywood, A.M., 2011, Persistent El Niño–Southern Oscillation variation during the Pliocene Epoch: Paleoceanography, v. 26, PA2215.

Seki, O., Foster, G.L., Schmidt, D.N., Mackensen, A., Kawamura, K., and Pancost, R.D., 2010, Alkenone and boron-based Pliocene pCO_2 records: Earth and Planetary Science Letters, v. 292, p. 201–211. DOI:10.1016/j.epsl.2010.01.037

Seki, O., Schmidt, D.N., Schouten, S., Hopmans, E.C, Sinninghe Damsté, J.S., and Pancost, R.D., 2012, Paleoceanographic changes in the Eastern Equatorial Pacific over the last 10 Myr: Paleoceanography, v. 27, PA3224.

Sepulchre, P., Arsouze, T., Donnadieu, Y., Dutay, J.C., Jaramillo, C., Le Bras, J., Martin, E., Montes, C., and Waite, A., 2014, Consequences of shoaling of the Central American Seaway determined from modeling Nd isotopes: Paleoceanography, v. 29, p. 176–189. DOI:10.1002/2013PA002501

Sinninghe Damsté, J.S., Hopmans, E.C., Schouten, S., Van Duin, A.C.T., and Geenevasen, J.A.J., 2002, Crenarchaeol: the characteristic core glycerol dibiphytanyl glycerol tetraether membrane lipid of cosmopolitan pelagic crenarchaeota: Journal of Lipid Research, v. 43, p. 1641–1651.

Spero, H.J., Mielke, K.M., Kalve, E.M., Lea, D.W., and Pak, D.K., 2003, Multispecies approach to reconstructing eastern equatorial Pacific thermocline hydrography during the past 360 kyr: Paleoceanography, v. 18, p. 1–16.

Srinivasan, M.S., and Sinha, D.K., 1998, Early Pliocene closing of the Indonesian Seaway: evidence from north-east Indian Ocean and Tropical Pacific deep sea cores: Journal of Asian Earth Sciences, v. 16, p. 29–44.

Steph, S., Tiedemann, R., Prange, M., Groeneveld, J., Schulz, M., Timmermann, A., Nürnberg, D., Rühlemann, C., Saukel, C., and Haug, G.H., 2010, Early Pliocene increase in thermohaline overturning: a precondition for the development of the modern equatorial Pacific cold tongue: Paleoceanography, v. 252, 17 p.

Takayama, T., 1993, Notes on Neogene calcareous nannofossil biostratigraphy of the Ontong Java Plateau and size variations of Reticulofenestra coccoliths, *in* Berger, W.H., Kroenke, L.W., Mayer, L.A., et al., eds., Ocean Drilling Program: Scientific Results, Proceedings, v. 130, p. 179–229.

Ternois, Y., Sicre, M.-A., and Paterne, M., 2000, Climatic changes along the northwestern African continental margin over the last 30 kyrs: Geophysical Research Letters, v. 27, p. 133–136.

Tian, B., Zhang, G.J., and Ramanathan, V., 2001, Heat balance in the Pacific warm pool atmosphere during TOGA COARE and CEPEX: Journal of Climate, v. 14, p. 1881–1893.

Tierney, J.E., and Tingley, M.P., 2015, A TEX_{86} surface sediment database and extended Bayesian calibration: Scientific Data, 2150029. DOI: 10.1038/sdata.2015.29

Tierney, J.E., and Tingley, M.P., 2018, BAYSPLINE: a new calibration for the alkenone paleothermometer: Paleoceanography and Paleoclimatology, v. 33, p. 281–301.

Timmermann, A., An, S.I., Krebs, U., and Goosse, H., 2005, ENSO Suppression due to weakening of the North Atlantic thermohaline circulation: Journal of Climate, v. 18, p. 3122–3139.

Wakeham, S.G., Peterson, M.L., Hedges, J.I., and Lee, C., 2002, Lipid biomarker fluxes in the Arabian Sea, with a comparison to the equatorial Pacific Ocean: Deep-Sea Research II, v. 49, p. 2265–2301.

Wakeham, S.G., Hopmans, E.C., Schouten, S., and Sinninghe Damsté J.S., 2004, Archaeal lipids and anaerobic oxidation of methane in euxinic water columns: a comparative study of the Black Sea and Cariaco Basin: Chemical Geology, v. 205, p. 427–442.

Wara, M.W., Ravelo, A.C., and Delaney, M.L., 2005, Permanent El Niño-Like Conditions During the Pliocene Warm Period: Science, v. 309, p. 758–761.

Williams, T., Van De Flierdt, T., Hemming, S.R., Chung, E., Roy, M., and Goldstein, S.L., 2010, Evidence for iceberg armadas from East Antarctica in the Southern Ocean during the late Miocene and early Pliocene: Earth and Planetary Science Letters, v. 290, p. 351–361.

Woodruff, F., and Savin, S.M., 1989, Miocene deep water oceanography: Paleoceanography, v. 4, p. 87–140.

Wuchter, C., Schouten, S., Wakeham, S.G., and Sinninghe Damsté, J.S., 2005, Temporal and spatial variation in tetraether membrane lipids of marine Crenarchaeota in particulate organic matter: implications for TEX_{86} paleothermometry: Paleoceanography, v. 20, PA3013.

Yin, J.H., and Battisti, D.S., 2001, The importance of tropical sea surface temperature patterns in simulations of Last Glacial Maximum climate: Journal of Climate, v. 14, p. 565–581.

Zhang, Y.G., Pagani, M., and Liu, Z., 2014, A 12-million-year temperature history of the tropical Pacific Ocean: Science, v. 344, p. 84–86.

Received 30 April 2018; accepted 19 December 2018.